Available online at www.sciencedirect.com

ScienceDirect

International Journal of Thermal Sciences 48 (2009) 815–824

International Journal of Thermal Sciences

www.elsevier.com/locate/ijts

Performance characteristics of pulsating heat pipes as integral thermal spreaders

Honghai Yang [a], Sameer Khandekar [b,*], Manfred Groll [c,1]

[a] College of Environmental Science and Engineering, Donghua University, Shanghai 200051, PR China
[b] Department of Mechanical Engineering, Indian Institute of Technology Kanpur, Kanpur 208016, India
[c] Panorama Street 50, D-70839 Gerlingen, Germany

Received 7 September 2007; received in revised form 4 February 2008; accepted 27 May 2008

Available online 24 June 2008

Abstract

In the recent past, Pulsating Heat Pipes (PHPs) have attracted the attention of many researchers as viable candidates for enhanced heat transfer through passive two-phase heat transfer mechanism. Although a complete theoretical understanding of operational characteristics of this device is not yet achieved, there are many emerging niche applications, ranging from electronics thermal management to compact heat exchangers. For a better theoretical understanding, it is vital to generate experimental data under various operating boundary conditions. In this background, this paper presents an experimental study on two flat plate closed loop pulsating heat pipes in a thermal spreader configuration. Both are made of aluminum with overall size $180 \times 120 \times 3$ mm^3; one structure having 40 parallel square channels with cross-section 2×2 mm^2, while the second with 66 parallel square channels with cross-section 1×1 mm^2. The working fluid employed was Ethanol. Some peculiar performance trends, in comparison with circular channel devices, have been observed which are attributed to the sharp angled corners of the channels. The influence of various operating parameters, including volumetric filling ratio of the working fluid, input heat flux and operating orientation, on the thermo-hydrodynamic performance, was investigated. Successful operation at all orientations with respect to gravity was also achieved. In terms of applications, this paper explores the possibility of embedded pulsating heat pipe as an integrated structure or heat spreader, so as to render higher overall thermal conductance to the host substrate.

Keywords: Flat plate closed loop pulsating heat pipes; Self-sustained thermally driven oscillations; Heat spreaders; Thermal performance; Two-phase flow patterns

1. Introduction

Electronics thermal management can be subdivided into three levels as elaborated in Fig. 1. While on level-1, cooling is typically achieved by conduction/diffusion process combined with proper choice of materials, two-phase passive heat transfer cooling technology is steadily finding its way on level-2 and level-3 [1,2]. Conventional mini/micro heat pipes are already serving the industry needs and can be found in many present day thermal management strategies for laptop computers, servers and power electronic components [3–5]. In general, there is an ongoing effort to combine functional components and thermal spreaders on the chip level itself thereby integrating the management strategies for level-2 and level-3 [6]. This can substantially contribute towards the contemporary trend of miniaturization.

Pulsating Heat Pipes (PHPs) are passive heat transfer devices consisting of meandering continuous tube bundles/flow passages of capillary dimensions in which a two-phase mixture of a working fluid exists. This mixture undergoes self-excited oscillations when subjected to a thermal gradient (for specific detailed information on constructional/operational features, please refer [7–9]). PHPs have already found applications in cooling of power/microelectronic components but not many studies exist on the feasibility of these devices as integrated heat spreaders on a circuit/substrate interface level. This will typically necessitate flat plate structures having dimensions as

* Corresponding author. Tel.: +91 512 259 7038; fax: +91 512 259 7408.
E-mail address: samkhan@iitk.ac.in (S. Khandekar).

[1] Formerly at IKE, University of Stuttgart, 70569 Stuttgart, Germany. Visiting Professor at IIT Kanpur, India, from January–March 2008.

1290-0729/$ – see front matter
doi:10.1016/j.ijthermalsci.2008.05.017

Nomenclature

A	area	m^2
Bo	Bond number $= D((g(\rho_{liq} - \rho_{vap})/\sigma)^{0.5})$	
D	diameter	m
d	groove depth	m
FR	filling ratio (V_{liq}/V_{tot}) at room temperature	
g	acceleration due to gravity	m/s^2
L	length	m
l	groove length	m
N	number of grooves	
P	electrical power	W
$\dot{Q}$	heat power	W
q''	heat flux	W/m^2
R_{th}	thermal resistance	K/W
T	temperature	°C or K
t	time	s
V	volume	m^3
w	groove width	m

Greek symbols

σ	surface tension	N/m
ρ	density	kg/m^3

Subscripts

ad	adiabatic
ax	axial
c	condenser
crit	critical
e	evaporator
hyd	hydraulic
liq	liquid
loss	heat loss
rad	radial
tot	total
vap	vapor

Abbreviations

CLPHP	Closed Loop Pulsating Heat Pipe
PHP	Pulsating Heat Pipe

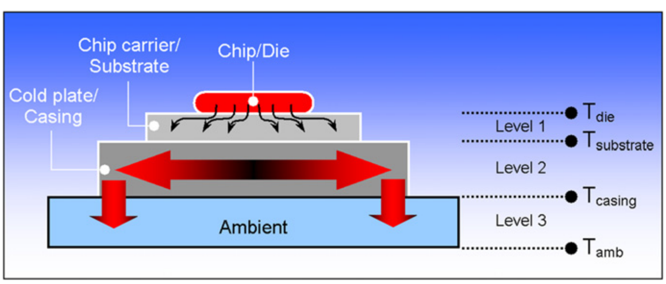

Fig. 1. Thermal management levels of a typical electronics package.

applicable for multi-chip modules or printed circuit boards. Another potential application of such embedded integrated PHP structures could be in the form of thermal spreaders under conjugate convective conditions (terrestrial applications) or under pure radiative boundary conditions (space applications; for example see [10]). This seems to be the next logical step for widening the application area of pulsating heat pipes.

Functional operation of a PHP is multivariate; its performance is affected by complex interplay of many parameters and there is a strong thermo-hydrodynamic coupling governing its performance. In the last decade, various performance and characterization studies have been undertaken; six major parameters have emerged as the primary influence parameters affecting the system dynamics [8,11–19]. These include:

– Internal diameter of the CLPHP tube,
– Volumetric filling ratio of the working fluid,
– Input heat flux,
– Total number of turns,
– Device orientation and,
– Thermo-physical properties of the working fluid.

Literature also suggests that the net heat transfer achieved is a combination of the sensible heat transport through liquid plugs and latent heat transfer through the vapor bubbles. If the internal flow pattern remains predominantly in the slug flow regime, then the latent heat does not play a dominant role in the over-all heat transfer. If there is transition to annular flow under the imposed thermo-mechanical boundary conditions, then the dominance of latent heat increases. The following are some of the characteristics features of PHPs [8]:

– Depending on the size and operating boundary conditions, PHPs may be better or worse than conventional wicked heat pipes of equivalent sizes, in terms of overall thermal resistance and/or axial heat transport capability under normal operating conditions. At the least, manufacturing complexities of conventional heat pipes, especially for mini/micro scale application, are avoided in PHPs. In addition, the near orientation-independent operating characteristic is another attractive feature in favor of PHPs.
– As compared to solid metallic fins, there is a considerable weight advantage in case of PHPs. Needless to mention, the thermal superiority of PHPs as compared to solid fins, provided they operate satisfactorily.
– As compared to an equivalent single-phase forced convection liquid cooling option, PHPs are attractive not only for pressure drop penalty considerations in the former case, but also for the passivity and reliability they render to the cooling system.

PHPs loose their fundamental character (self-sustained thermally driven oscillating flows) if certain boundary conditions

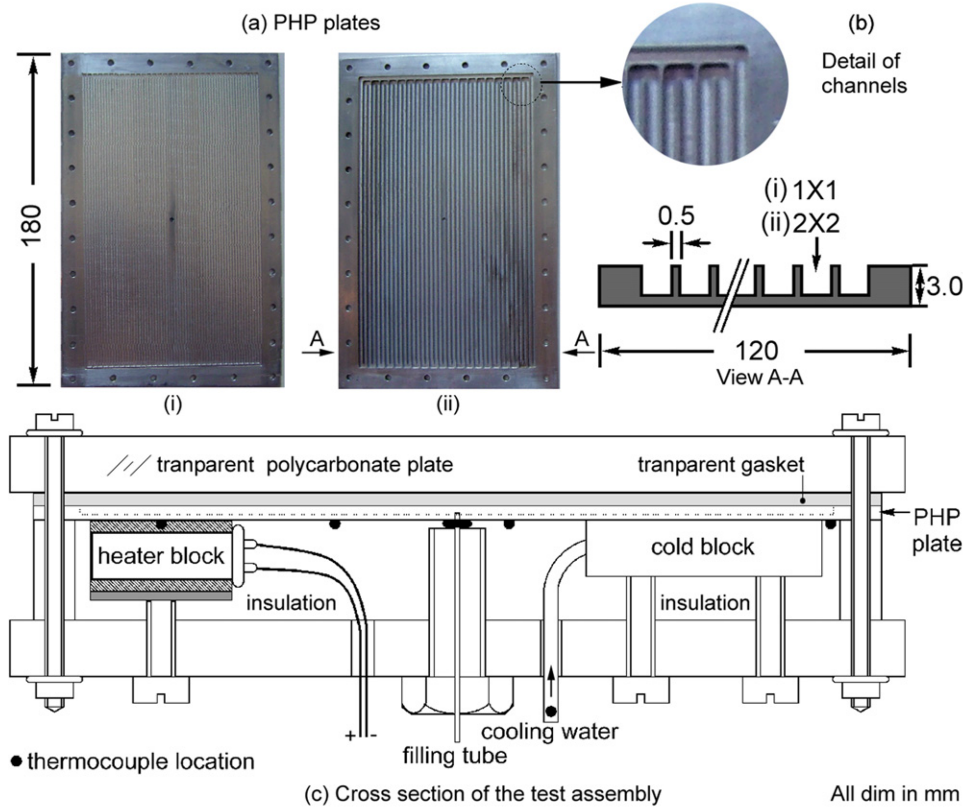

Fig. 2. Details of the experimental setup. (a) Photographs of the PHP substrates, (b) details of the channels, (c) cross-section of the setup assembly.

pertaining to input heat flux and filling ratio are not satisfied. Following parameters/conditions affect the range of internal two-phase flow instabilities of PHPs and the characteristic flow patterns emanating from them, which, in turn, affect the performance:

- Geometrical Parameters: Channel/tube size, number of channels.
- Operating Conditions: Orientation; external body force field, system pressure.
- Boundary Conditions: Applied heat flux/temperature level distribution, cooling conditions.

Compatibility with PHP material, thermal stability, wettability, favorable vapor pressure gradient, high latent heat, low liquid/vapor viscosities and acceptable freezing point are the few parameters which do effect the selection criteria of a suitable working fluid. At present, there is no explicit figure of merit available for choosing the working fluid to rationalize the effect of thermophysical parameters on the performance of the device. This remains an active area of investigation.

In general, since many thermo-mechanical parameters affect the system performance, there is a need to undertake experimental studies to evaluate the performance of different PHP designs under diverse operating conditions, not only to aid fundamental understanding but also for exploring potentially new applications. In this background, the present study focuses attention on the generic design of rectangular aluminum plates engraved/machined with PHP flow structures on them. Such devices may find application as substrates for direct integration with electronics components (level 2) or as spreader/radiator plates for satellite application (level 3). Other applications include power electronics thermal management and as casing/structural components for electronics packages (hybrid level 2/3).

2. Experimental setup and methodology

The details of the experimental setup are shown in Fig. 2. Two PHP test sections were fabricated from aluminum plates with overall size $180 \times 120 \times 3\ mm^3$. PHP spreader #1 had a total of 66 parallel interconnected rectangular channels forming a meandering closed loop (cross-section $1 \times 1\ mm^2$, length per tube 165 mm). PHP spreader #2 was also closed loop and had a total of 40 parallel square channels (cross-section $2 \times 2\ mm^2$, length per tube 165 mm). A polycarbonate backing plate with a thin transparent silicon sheet tightly covered the top of PHP spreader to allow visualization of the internal thermofluiddynamic phenomena from above. A copper heater block ($100 \times 30 \times 15\ mm^3$) employing three embedded cartridge AC heaters (ϕ 10×25 mm) constituted the heat source. A cold copper block ($100 \times 60 \times 12\ mm^3$), always supplied with 20 °C water, acted as the heat sink. These blocks were attached respectively on the back face of each PHP spreader; the area between the heater and cooling block formed the adiabatic section, where a vacuum/filling tube was provided, as shown.

For temperature measurements, ungrounded sheathed thermocouples ($D = 0.5$ mm, Type-K, Thermacoax®, accuracy ±0.2 °C after calibration) were used. Three were symmetrically

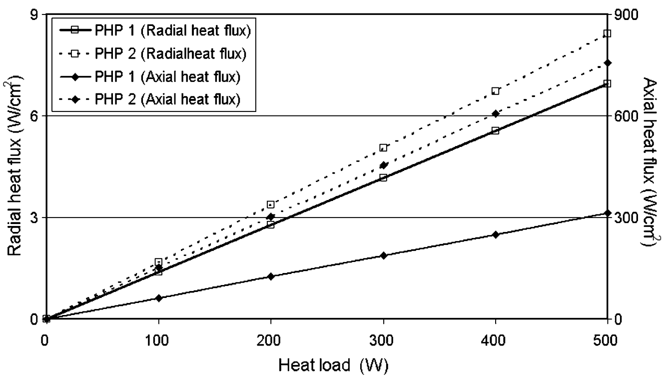

Fig. 3. Applicable variation of radial and axial fluxes with applied heat power input in the present experimental setup.

located in the heater section, three were attached to the spreader surface at the end of the condenser section, and another two were located in the adiabatic section along the center line, as depicted in Fig. 2.

Ethanol was used as the working fluid. The Filling Ratio (FR, defined as the ratio of the liquid volume enclosed in the channel loop to the total loop volume, at room temperature) ranged from 5% to 95%. The thermal resistance of the dry structure (FR = 0%) was also measured for baseline comparison. Three heating configurations were investigated, viz. bottom heat orientation (+90°), horizontal heat (0°) and top heat orientation (−90°) respectively.

The PHP performance data (for each filling ratio and each inclination angle) were obtained according to the following procedure: Heat input was stepwise increased until a quasi thermal equilibrium was established. Then, the spatial temperatures and heat input were recorded, so the thermal resistances could be determined. The procedure was repeated till an average evaporator temperature $\bar{T}_e$ (see Eq. (2)) of about 110 °C, corresponding to safe setup operation, was reached. The thermal resistance is defined, as usually done, by

$$R_{th} = (\bar{T}_e - \bar{T}_c)/\dot{Q} \tag{1}$$

where, $\bar{T}_e$ and $\bar{T}_c$ are the average evaporator and condenser surface temperatures, defined as,

$$\bar{T}_i = (T_{i,1} + T_{i,2} + T_{i,3})/3, \quad i = \text{e or c} \tag{2}$$

$\dot{Q}$ is heat input power to the PHP, which is transported from evaporator to condenser. Considering thermal losses, $\dot{Q}$ can be determined by:

$$\dot{Q} = P - \dot{Q}_{loss} \tag{3}$$

where P is the input electrical power (measured with accuracy of ±1.5%). $\dot{Q}_{loss}$ is the heat loss, which was verified to be about 4% to 9%, depending on the heat load.

The radial heat flux in the evaporator and the axial heat flux transported from evaporator to condenser are determined by

$$q''_{rad} = \dot{Q}/A_{rad} \quad \text{where } A_{rad} = N(2d + w) \cdot l_e \tag{4}$$

$$q''_{ax} = \dot{Q}/A_{ax} \quad \text{where } A_{ax} = Ndw \tag{5}$$

The variation of the respective heat fluxes with input heat power, as applicable for the present range of experiments, is given in Fig. 3.

3. Results and discussion

In general, both PHP spreaders could be successfully operated in all orientations and showed good thermal performance. Although the qualitative behavior of both the spreaders was similar, as PHP spreader #2 with the larger grooves had an overall better performance than PHP spreader #1 (detailed comparison done later, refer Section 3.5), the results for PHP spreader #2 are discussed first in more detail. Qualitatively, the discussion is applicable for both spreaders.

3.1. *Effect of tube cross-section*

Before proceeding to the actual performance results, it is worthwhile to discuss the effect of the tube cross-section on the operational characteristics of pulsating heat pipes. Comparing a circular channel of diameter D and a square section of side $= D$, although we notice that the hydraulic diameter of both the geometries is equal ($= D$), the volume per unit length of the latter geometry is $(4/\pi)$ times the former. Thus, if we make two PHPs with circular and square sections having the same hydraulic diameter, there will be a fundamental difference in their operating characteristics.

Referring to Fig. 4, if a square cross-section channel is filled below FR ≈ 22%, then all the liquid will tend to accumulate in the corners. This gives rise to some capillary action generated due to sharp angled corners. The menisci recede to lower radii of curvature if the filling ratio is made less than 22%, improving the capillary action of the sharp corners of the cross-section. On the contrary, such a phenomenon is not expected in a circular channel, although both have the same hydraulic diameter. If we fill the circular cross-section capillary tube, whose diameter is comparable to or less than the critical diameter specified by the Bond number criterion (see Eq. (6) below) with, say 10% liquid, then the probability of distinct liquid plug formation is definitely much higher than for the equivalent square cross-section channel. Similar arguments can be given for an equivalent triangular cross-section tube, wherein all the liquid tends to accumulate in the corners if FR ≈ 39.5% or less, as shown in Fig. 4(c). Furthermore, in the background of the ongoing discussion, it is self-evident that the critical diameter governed by the Bond number, as given by Eq. (6) below, is rather inappropriate for the case of channels with sharp angled corners.

$$D_{crit} \leqslant 2 \cdot \left[\frac{\sigma}{(\rho_{liq} - \rho_{vap}) \cdot g}\right]^{1/2} \tag{6}$$

The shape also affects the flow regime transitions. The flow regimes/patterns are affected by the interplay of gravity, surface tension, shear and inertia forces. The relative magnitude of the forces is clearly affected by the absolute/hydraulic diameter of the tube cross-section as well as the shape. Thus, it is expected that the sharp corners of a square/triangular cross-section would allow the liquid phase to be readily trapped along the wetted perimeter. This may allow slug and annular flows to be sustained at higher liquid and gas superficial velocities [20]. A typical interface perturbation of a given magnitude will affect

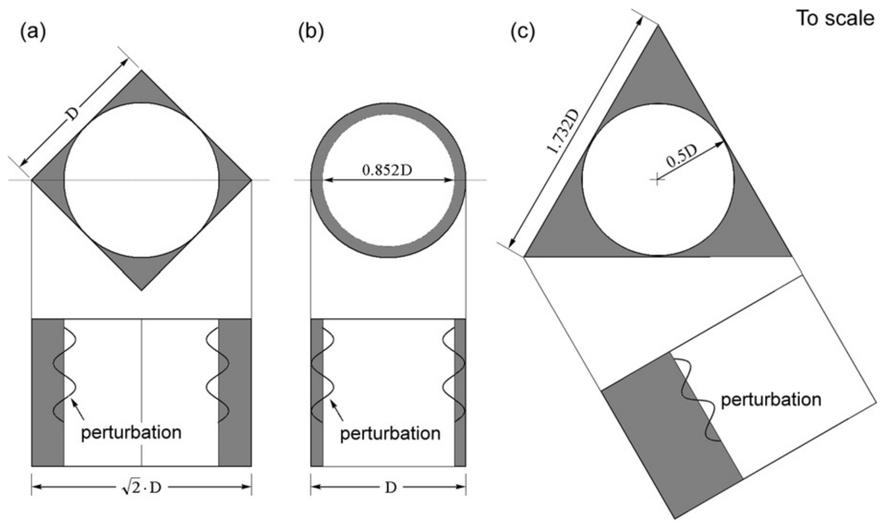

Fig. 4. Tubes having same hydraulic diameter but different cross-sectional shapes lead to dissimilar effects on thermo-hydrodynamics of a PHP. (a) Square, (b) circular and (c) triangular cross-section.

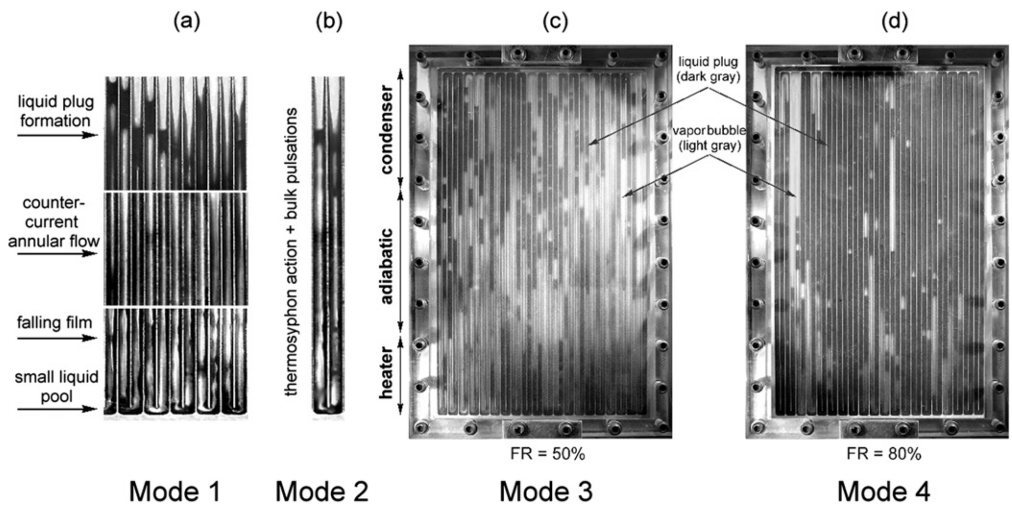

Fig. 5. Different modes of PHP operation. (a) Mode 1: Thermosyphon mode; (b) Mode 2: Combination of thermosyphon mode superimposed by intermittent pulsations; (c) Mode 3: True self sustained pulsating action; (d) Mode 4: Excess liquid condition with intermittent pulsations.

the square cross-section and circular cross-section in a different manner thus affecting Kelvin–Helmholtz type instabilities and flooding/bridging phenomena. The above noted peculiarities of a sharp angled PHP were also partly observed earlier by Khandekar et al. [21]. These are decisively confirmed by the results of the present study. Recently, Qu et al. have also tested mini PHPs with triangular and square sections [22].

3.2. Characteristic modes of PHP operation

The two parameters, i.e. filling ratio and heat load, cannot be dealt with separately since they simultaneously affect the internal two-phase flow patterns thereby dictating the dominant heat transfer mechanism and thus the performance. Based on our experimental observations, we categorize the device performance in primarily four major operating modes, as described below.

3.2.1. Mode-1

Thermal resistance for the dry device is ≈ 3 K/W. When the filling ratio is low ($<\approx 20\%$), the spreader behaves as an interconnected array of two-phase thermosyphons. Obviously, it can only operate in the bottom heat orientation. This operation mode is unique to the sharp angled cross-section and was not distinctly observed in previous studies with circular cross-section PHPs. The reasons have been explained in the previous section. Fig. 5(a) captures the flow pattern details in this mode of operation, wherein the operation is similar to an interconnected array of two-phase thermosyphons. Application of heat results in a ‘nucleate pool boiling’ type scenario in the individual evaporator U-turns. Slowly, counter-current annular flow develops in individual channels. Vapor flows upwards in every channel and condensate flows down in ripple/rivulet flow. As the vapor condenses, sometimes flooding/bridging is observed, resulting in the formation of distinct liquid plugs. These plugs eventually drain down the channel walls through the sharp angled corners. Thus, a ‘pseudo’ counter-current flow, occasionally interrupted by formation of bridged liquid plugs, is well established. There are little observable bulk pulsations/oscillations; although intermittently, instabilities are observed due to the interconnected nature of the thermosyphon array. As the heat load is further increased, the device tends quickly towards a dry-out.

3.2.2. Mode-2

This mode with FR $\approx$ 20% to 40% represents the transition from the classical thermosyphon mode just described to a pulsating capillary slug flow regime. The fluid phases start migrating to adjacent channels and well defined counter-current flow of the two-phases tends to get disrupted due to the presence of more liquid plugs. Increase in filling ratio will further reduce the distinct thermosyphon effect. Now, the spreader can operate well, both in the bottom heat and horizontal heat orientation, but almost cannot operate in the top heat orientation.

In the case of bottom heat orientation, the flow pattern is a mixture of classical thermosyphon type counter-current annular flow in some channels and capillary slug flow in others, as depicted in Fig. 5(b). There are instances when condensate return is seen as liquid thin film flowing downwards. In addition, there is also a sustained period of capillary slug flow, involving a group of adjacent interconnected channels. Thus, a combination of flow patterns exists. In contrast, in the case of horizontal heat orientation, the only dominant flow regime is capillary slug flow (as gravity assisted thermosyphon action is not possible). The plugs/bubbles primarily oscillate in individual channels of the device.

3.2.3. Mode-3

When the filling ratio is between about 40% and 70%, the spreader can operate rather well at all inclination angles (quantitative results are presented in later sections). The effect of the gravity vector becomes relatively insignificant. This mode represents the true pulsating heat pipe operation and is the most effective mode with respect to the thermal performance.

Self-sustained oscillating slug flow is the predominant flow pattern for horizontal and anti-gravity operation, irrespective of the heat input. At relatively higher heat loads, the oscillating slug flow gets intermittently superimposed by bulk circulation of the fluid, involving all the interconnected channels. This bulk circulation happens more and more as the heat load is increased thereby reducing the thermal resistance. During bulk circulation phase, adjacent tubes become 'upheaders' and 'downcomers' with alternatively hot and cold fluid mixtures flowing through them [21]. At small heat loads, individual liquid plugs only oscillate about a mean position along the channel length; there is little liquid plug agglomeration.

The flow pattern in the bottom heat orientation is most affected by the heat input. At low heat inputs, the flow pattern is predominantly oscillating slug flow and the evaporator temperature somewhat fluctuates (refer more details in later sections). There are periods in which the fluid movement drastically reduces and then all of a sudden there are violent oscillations coupled with bulk circulation which cools the evaporator. Increasing the heat throughput, further smoothens the operation as the evaporator U-sections experience sustained convective boiling, leading to churn, semi-annular and annular flow in many channels. Bulk circulation, as described earlier, is also superimposed. These combinations of events increase the local heat transfer coefficient and the performance is most desirable in such a situation. A typical snap-shot of a 50% filled device in such an operating mode is shown in Fig. 5(c).

3.2.4. Mode-4

When filling ratio is more than 70%, there is excess liquid which reduces the degree of freedom of the system and the effective advantage of the sharp angled corners. It is almost impossible for the vapor to reach the condenser area unhindered without encountering liquid plugs on the way. A typical snap-shot of a 80% filled device operating in bottom heat orientation is shown in Fig. 5(d). Oscillating/pulsating action markedly decreases and even disappears for extended time periods. The spreader cannot operate in the top heat orientation. If the spreader can operate in the horizontal heat orientation (normally, operation is not always guaranteed), oscillating slug flow is the only flow pattern. In the case of bottom heat orientation, nucleate boiling also occurs in the evaporator section, resulting in the formation of small bubbles. The degree of fluid oscillations is the maximum in the bottom heat orientation. Still, the overall operation is not quite satisfactory.

For FR = 100% the system works as a single phase thermosyphon [23]. For the present experiment it was not possible to fill it 100% due to inherent vapor flashing which could not be avoided.

3.3. Oscillations of evaporator temperature

Fig. 6 shows the typical evaporator temperature-time history at different heat power input and operating orientations (T: Top heat; H: Horizontal; B: Bottom heat orientation) for PHP spreader #2. The fill charge for these tests is 55% wherein the PHP operates in Mode-3. Many interesting features can be noted from these trends:

(i) For all orientations, the average amplitude of oscillations in the evaporator temperature decreases with increasing power input and vise-versa.
(ii) In the entire range of input heat power, the average amplitude of evaporator temperature oscillations is higher for Top heat orientation followed by Horizontal orientation and the least for Bottom heat orientation. Lower the amplitude, more uniform and less intermittent are the internal fluid flow oscillations.
(iii) For a given heat input power, the average evaporator temperature is lowest for the bottom heat orientation. In other words, for a fixed maximum safe evaporator temperature, more heat can be transferred in bottom heat orientation.
(iv) In the intermediate power input range, comparable performance is obtained at all orientations.

Many of these observations are in line and complimentary with the observations made by other groups reporting on operating characteristics of PHPs (for example [11,12,18,19]).

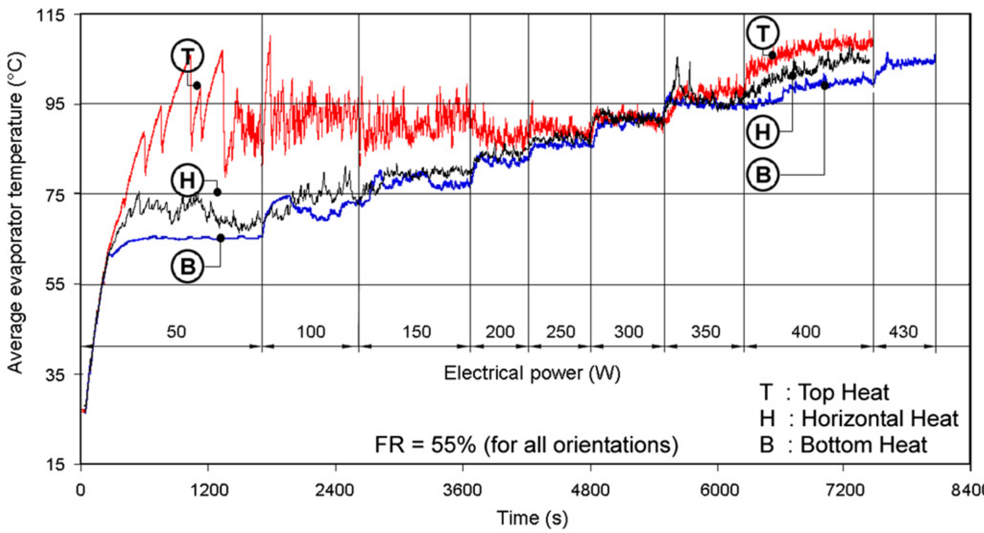

Fig. 6. Typical temporal variation of evaporator temperature for the 2 × 2 mm^2 PHP at different heat input power levels and FR = 55%.

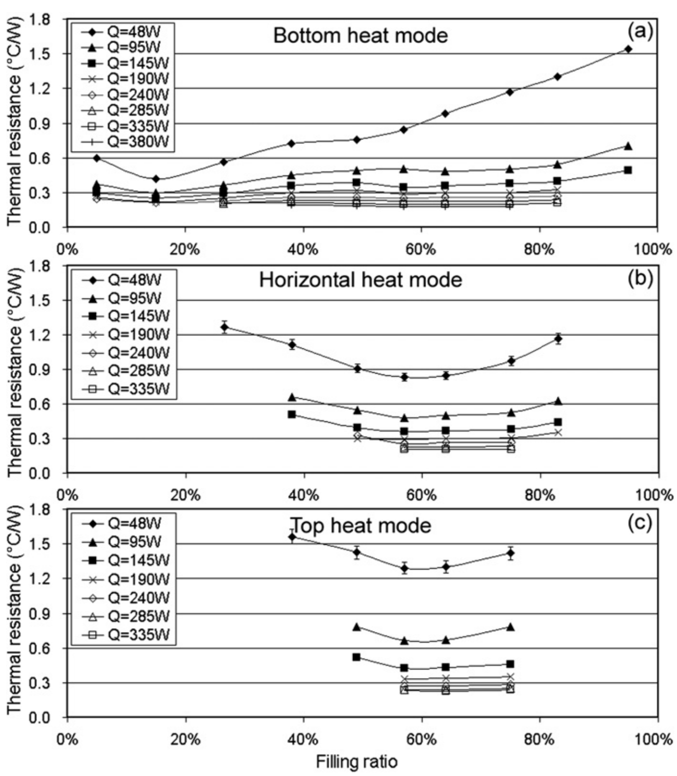

Fig. 7. Effect of filling ratio on the thermal resistance of the 2 × 2 mm^2 PHP. (a) Bottom heat orientation, (b) horizontal heat orientation, (c) top heat orientation.

3.4. *Effective thermal performance*

Fig. 7 shows the thermal performance of PHP spreader #2 in terms of effective thermal resistance for a given input heating power with varying filling ratios. In the bottom heat orientation, the spreader could operate within a wide filling ratio range from 5% to 95%. In the horizontal orientation, the operational range was from FR = 30% to 85%, and in the top heat orientation the operational range become narrower, viz. 45% to 75%. Also, as can be seen, in bottom heat orientation at low heat input, two local minima are observed. At FR ≈ 15%, the first dip comes under Mode-1 operation and corresponds to the gravity thermosyphon effect, as explained earlier. The sharp angled corners distinctly produce capillarity which enhances the thermosyphon effect. With increasing heat power input, Mode-1 action terminates due to thermosyphon dryout. The second minimum corresponds to Mode-3. Here, the combined effect of bubble pumping coupled with favorable oscillating flow pattern governs the heat transfer. It is worth noting that, on one hand, the thermal resistance in Mode-1 (thermosyphon mode) is smaller than that in Mode-3, but on the other hand, maximum heat throughput in the former mode is restricted by counter-current flow limitation leading to eventual dry-out. As can be clearly seen, the sensitivity of filling ratio as an influencing parameter gets reduced with increasing heat load. Similar trends are recorded for horizontal heat orientation also. For top heat orientation, the device can only operate primarily under Mode-3.

Fig. 8 depicts essentially the same data points as Fig. 7 but is presented here for clarity and better perspective. It shows the effect of heat input on the thermal resistance. It is found that increasing heat load markedly improves the thermal performance. Till about 200 W input the performance improvement is quite drastic while thereafter it is milder. This tendency is the same for all filling ratios and inclination angles. Overall, the trends are quite similar to other previous studies reported for other geometrical configurations of PHPs (for example [11–17]).

In general, the heat input is the ‘pump’ for the oscillatory thermo-fluidic action; thus, increasing ‘pumping power’ increases the performance. At low filling ratios (Mode-1: Thermosyphon mode and Mode-2: Transition), increasing heat input makes the liquid layer in the counter-current flow thinner. The effective fluid velocity also increases thus enhancing the local wall heat transfer coefficient. In Mode-3 operation, bubble pumping action gets enhanced due to rapid bubble growth (in the evaporator section) and collapse (in the condenser section). Also, after a certain heat input, the flow changes from purely capillary slug flow to churn/semi-annular and sometimes to fully annular flow in individual channels, as explained ear-

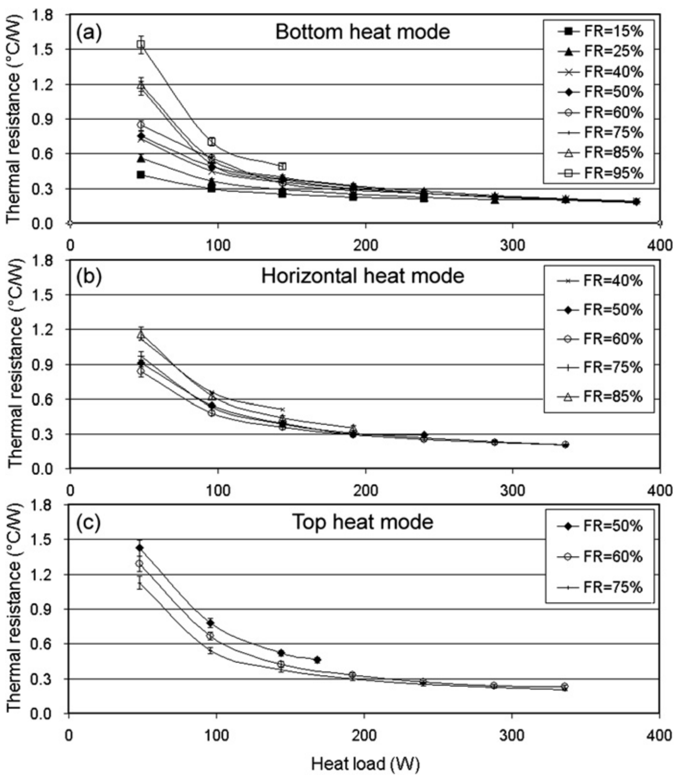

Fig. 8. Effect of input heat power on the thermal performance of the 2×2 mm^2 PHP. (a) Bottom heat orientation, (b) horizontal heat orientation, (c) top heat orientation.

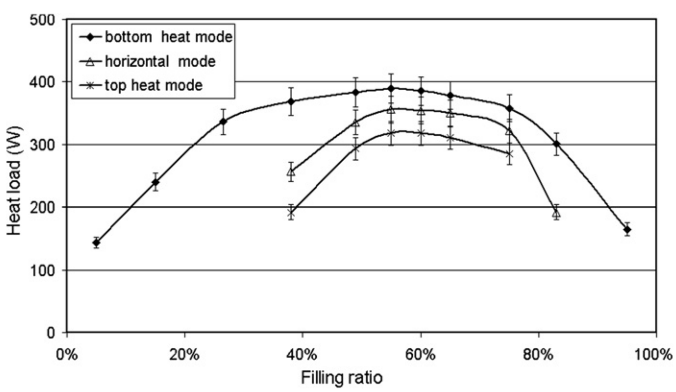

Fig. 9. Variation of maximum heat load for obtaining $\bar{T}_e \sim 110\,^\circ\mathrm{C}$ with respect to filling ratio of PHP spreader #2 (2×2 mm^2).

lier. This greatly enhances the heat transfer coefficient. Thus, increasing heat load will enhance the performance till a certain type of dry-out occurs. In Mode-1, the dry-out occurred as a combination of counter-current flow limitation and insufficient fluid inventory, starving some channels completely. In other modes, no dry-out could be observed. Experiments were terminated for safety reasons beyond $\sim 120\,^\circ\mathrm{C}$ local evaporator temperatures.

In Fig. 9, maximum heat throughput for an average evaporator temperature of $\approx 110\,^\circ\mathrm{C}$ are recorded for the three operating orientations ($-90°$, $0°$, $+90°$). It can be clearly seen that for the bottom heat orientation, the operationally viable filling ratio has a much wider range from 5% to 95%, and overall, the PHP

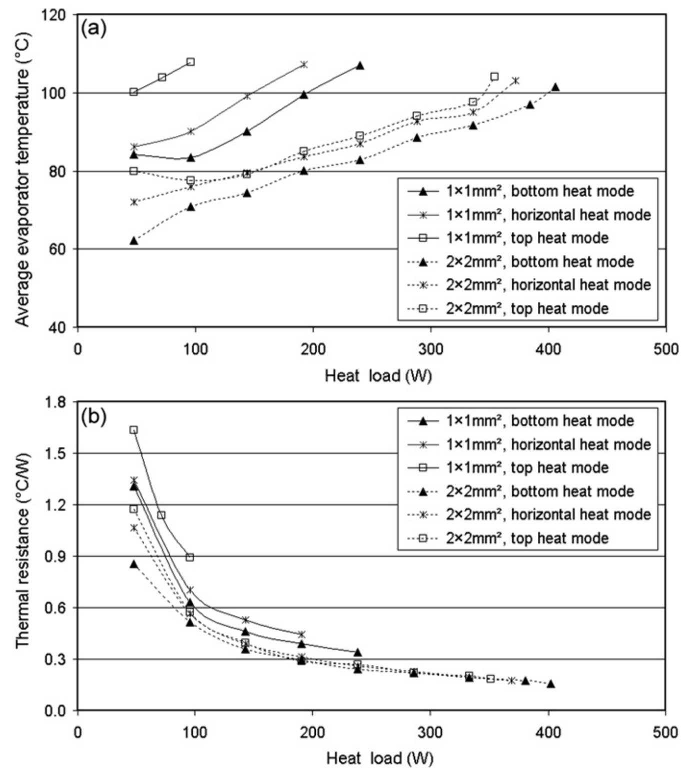

Fig. 10. Comparison of thermal performance of the two tested PHP spreaders. (a) Average evaporator temperature with supplied heating power (experiment stopped at $\bar{T}_e \sim 110\,^\circ\mathrm{C}$), (b) comparison of thermal performance at different heat input power.

allows higher heat throughputs for a fixed evaporator temperature. For filling ratios between 20% and 85% the maximum heat load is above 300 W. In the case of horizontal and anti-gravity top heat orientation, similar high heat loads can only be obtained for filling ratios in a relatively narrow range from about 45% to 75%, and about 50% to 70%, respectively. The maximum obtained heat throughput, keeping the average evaporator temperature at $100\,^\circ\mathrm{C}$, were 390 W for $+90°$, 360 W for $0°$, but 320 W for $-90°$. Thus, the gravity vector affects thermal performance. This effect can be minimized by the choice of proper filling ratio and input heat power.

3.5. Performance comparison of PHP spreader #1 and #2

In Fig. 10(a), (b) the thermal performance of PHP spreader #1 and PHP spreader #2 are compared for all operating orientations and FR $\approx 55\%$, which is approximately the optimum, in terms of overall performance.

If the overall size of two devices is comparable and the wall thickness between two adjacent channels is fixed, then a device having smaller cross-section will have a lesser fluid inventory. Moreover, since the gravitational driving head ($= g\Delta\rho L$) will be the same for both the devices, the frictional handicap for the smaller channel size device should render it less effective. These arguments are based on the fact that gravity is the only driving force which has to overcome the two-phase frictional resistance. The very fact that PHPs are operating in the anti-gravity direction suggests that there is an additional driving force other than gravity. This driving force is supposed to come from the bubble growth and collapse process. The quantification of this force has still not been properly achieved [24]. In this background we present here comparative results of the two thermal spreaders. More work is needed in this direction. As can be seen, PHP spreader #2 with the bigger channel size had a better thermal performance (maximum heat load of about 390 W for PHP spreader #2 at $\bar{T}_e \approx 110\,^{\circ}\mathrm{C}$ vs. 200 W for PHP spreader #1 at the same average evaporator temperature). For a given load, PHP spreader #2 could be operated at lower evaporator temperatures and therefore smaller thermal resistances. The flow resistance (two-phase pressure drop) is markedly higher for spreader #1 thus hindering the overall heat throughput capacity at a given evaporator temperature. While this thermal spreader has a higher number of turns leading to more internal perturbations (in terms of higher number of instances of bubble growth and collapse), the increased flow resistance due to smaller channel size seems to seriously affect the thermal performance.

4. Summary and conclusions

Two aluminum flat plate closed loop pulsating heat pipes built as integrated thermal spreaders (overall size $180 \times 120 \times 3\ \mathrm{mm}^3$), with $D_{\mathrm{hyd}} = 1.0$ and 2.0 mm respectively, were tested under various operating conditions with ethanol as the working fluid. Major conclusions from the study are:

The cross-sectional shape of the device is an important parameter which affects not only the flow pattern transitions due to the effect of sharp angled corners, if present, it also has a bearing on the acceptable diameter of a PHP, as suggested by the critical Bond number criterion. Based on these observations, it can be argued that the Bond number criterion is not a blanket basis for choosing an operating diameter for the device; it only provides a tentative first order estimate.

The filling ratio is a critical parameter, which needs to be optimized to achieve maximum thermal performance and/or minimum thermal resistance for a given operating condition. For horizontal and top heat orientations, optimum filling ratio of about 50% – 65% was obtained, while in the bottom heat orientation the situation was more complex. For lower heat load range, an optimum filling of about 15%, corresponding to minimum thermal resistance, was obtained. This is attributed to the gravity assisted thermosyphon mode of operation, i.e. the device does not act as a PHP in this situation, but as an interconnected array of closed two phase thermosyphons. For higher heat loads, however, filling ratio has to be increased and the device starts to perform in self-excited thermally driven oscillating/pulsating mode. In this case, the maximum thermal performance is not very sensitive to FR in the range 40% – 70%.

Since the input heat load is the source of pumping action of the PHP, in general, increasing the heat load improves the performance. The mechanisms of a dry-out are not yet fully understood and only limited studies are available [25,26]. Due to safety reasons of the test specimen, dry-out phenomena and performance limitations could not be studied in the present work.

Though the two PHP spreaders could operate well in all orientations, the gravity vector does augment the driving forces, improving performance in the bottom heat orientation as compared to other orientations. While phenomenological operation of both the spreaders was similar, spreader #2 with bigger channel size ($2 \times 2\ \mathrm{mm}^2$) showed a considerably better thermal performance than PHP spreader #1 ($1 \times 1\ \mathrm{mm}^2$). This is attributed to higher two-phase dissipative losses in the latter geometry.

Acknowledgements

Financial support from Board of Research for Nuclear Sciences (BRNS), India, to the second author under the project IITK/BRNS/ME/20050292 is gratefully acknowledged. The first author received financial support from the German Academic Exchange Service (DAAD) and the China Scholarship Council. The last author wishes to thank IIT Kanpur, India, for inviting him as a visiting professor during January–March 2008.

References

[1] A. Bar-Cohen, Trends in packaging of computer systems, in: S. Kakac, H. Yüncü, K. Hijikata (Eds.), Cooling of Electronic Systems, Kluwer Academic Publishers, 1994, pp. 17–45.
[2] R.K. Ulrich, W.D. Brown (Eds.), Advanced Electronic Packaging, IEEE Press Series on Microelectronic Systems, ISBN-10:0471466093, 2006.
[3] M. Groll, M. Schneider, V. Sartre, M.C. Zaghdoudi, M. Lallemand, Thermal control of electronic equipment by heat pipes, International Journal of Thermal Science 37 (1998) 323–352.
[4] M. Groll, S. Khandekar, Heat transfer and fluid flow in microchannels: Micro heat pipes, in: G.F. Hewitt (Ed.), HEDH: Heat Exchanger Design Handbook-2002, Begell House, ISBN-10:1567001815, 2002.
[5] L.L. Vasiliev, Heat pipes in modern heat exchangers, Applied Thermal Engineering 25 (2005) 1–19.
[6] R. Mongia, M. Kuroda, H. Pokharna, Heat pipe needs in future mobile platforms, in: Proc. 14th International Heat Pipe Conference (IHPC), Florianopolis, Brazil, 2007.
[7] H. Akachi, US patent, Number 5490558, 1996.
[8] S. Khandekar, Thermo-hydrodynamics of closed loop pulsating heat pipes, Doctoral dissertation, Universitaet Stuttgart, Germany, 2004. Available at – http://elib.uni-stuttgart.de/opus/volltexte/2004/1939/.
[9] D. Reay, P. Kew, Heat Pipes, fifth ed., Butterworth–Heinemann, 2006, ISBN 10:0750667540.
[10] S. Khandekar, A. Gupta, Embedded pulsating heat pipe radiators, in: Proc. 14th International Heat Pipe Conference (IHPC), Florianopolis, Brazil, 2007.
[11] B.Y. Tong, T.N. Wong, K. Ooi, Closed-loop pulsating heat pipe, Applied Thermal Engineering 21 (18) (2001) 1845–1862.
[12] Y. Zhang, A. Faghri, Heat transfer in a pulsating heat pipe with open end, International Journal of Heat and Mass Transfer 45 (2002) 755–764.
[13] Q. Cai, C.L. Chen, J.F. Asfia, Operating characteristic investigations in pulsating heat pipe, Journal of Heat Transfer 128 (12) (2006) 1329–1334.
[14] S. Khandekar, M. Groll, An insight into thermo-hydraulic coupling in pulsating heat pipes, International Journal of Thermal Sciences 43 (1) (2004) 13–20.
[15] J.L. Xu, Y.X. Li, T.N. Wong, High speed flow visualization of a closed loop pulsating heat pipe, International Journal of Heat and Mass Transfer 48 (2005) 3338–3351.
[16] S. Khandekar, N. Dollinger, M. Groll, Understanding operational regimes of pulsating heat pipes: An experimental study, Applied Thermal Engineering 23 (6) (2003) 707–719.
[17] M.B. Shafii, A. Faghri, Y. Zhang, Thermal modeling of unlooped and looped pulsating heat pipes, Journal of Heat Transfer 123 (2001) 1159–1172.

[18] L. Lin, Experimental investigation of oscillation heat pipes, Journal of Thermophysics and Heat Transfer 15 (2001) 395–400.

[19] P. Charoensawan, S. Khandekar, M. Groll, P. Terdtoon, Closed loop pulsating heat pipes. Part A: Parametric experimental investigations, Applied Thermal Engineering 23 (16) (2003) 2009–2020.

[20] V.P. Carey, Liquid Vapor Phase Change Phenomena, second ed., Taylor and Francis, 2007.

[21] S. Khandekar, M. Schneider, P. Schaefer, R. Kulenovic, M. Groll, Thermofluiddynamic study of flat plate closed loop pulsating heat pipes, Microscale Thermophysical Engineering 6 (4) (2002) 303–318.

[22] W. Qu, Y. Zhou, Y. Li, T. Ma, Experimental study on mini pulsating heat pipes with square and regular triangle capillaries, in: Proc. 14th International Heat Pipe Conference (IHPC), Florianopolis, Brazil, 2007.

[23] S. Khandekar, M. Groll, P. Charoensawan, P. Terdtoon, Pulsating heat pipes: Thermo-fluidic characteristics and comparative study with single phase thermosyphon, in: Proc. 12th Int. Heat Transfer Conf., vol. 4, Grenoble, France, 2002, pp. 459–464.

[24] S. Khandekar, M. Groll, Insights into the performance modes of closed loop pulsating heat pipes and some design hints, in: Proc. 18th National & 7th ISHMT-ASME Heat and Mass Transfer Conference, Guwahati, India, 2006.

[25] H. Yang, S. Khandekar, M. Groll, Operational limit of closed loop pulsating heat pipes, Applied Thermal Engineering 28 (1) (2008) 49–59.

[26] P. Sakulchangsatjatai, N. Kammuanglue, P. Terdtoon, D.J. Mook, Effect of geometrical sizes on maximum heat flux of a vertical closed loop pulsating heat pipe, in: Proc. 14th International Heat Pipe Conference (IHPC), Florianopolis, Brazil, 2007.